2021 43rd Annual International Conference of the
IEEE Engineering in Medicine & Biology Society (EMBC)
Oct 31 - Nov 4, 2021. Virtual Conference

Geometry Factor Determination for Tetrapolar Impedance Sensor Probes

Carina Veil[1], Raphael Bach, Peter Somers[1], Oliver Sawodny[1], and Cristina Tarín[1]

***Abstract*— Even after successful tumor resection, cancer recurrence remains an important issue for bladder tumors. Intraoperative tissue differentiation can help for diagnostic purposes as well as for ensuring that all cancerous cells are completely removed, therefore, decreasing the risk of recurrence. It has been shown that the electrical properties of tumors differ from healthy tissue due to an altered physiology. This work investigates three sensor configurations to measure the impedance of tissue. Each relies on a four terminal measurement and has a distinct electrode arrangement either inline or as a square. Analytical expressions to calculate the geometry factor of each sensor based on Laplace's equation are derived. The results are verified experimentally and in a finite element simulation. Furthermore, several measurements on pig bladders, both fresh and from frozen storage, are carried out with each sensor.**

It is shown that the calculated and simulated geometry factors yield the same results and are suitable and uncomplicated methods to determine the geometry factor without an experimental setup. These methods also allow for sensor optimization by knowing the measured potentials before the actual fabrication of the sensor. Moreover, conductivity values close to listed data are obtained for pig bladders, which validates the sensors. Ultimately, the square electrode configuration turns out to be a valid option for minimally invasive sensors, which are necessary for the envisaged application of transurethral bladder cancer diagnostics and surgery. This arrangement both assures reliable data and allows for easier miniaturization than the inline electrode placement.

I. Introduction

Bladder cancer ranks among the most common cancers for men over 55 [1], and its long-term treatment is complicated by the elevated recurrence rate. A study conducted by Witjes et al. [2] in 2010 showed a recurrence rate of $40\,\%$ after transurethral bladder cancer resection. This is primarily due to the fact that the entity of tumor cells is not removed, mainly because the surgeon only has limited visual information during surgery. Additionally, with the bladder wall being rather thin, a generous resection of adjacent tissue is usually not possible.

Mainly, cancerous tumors differ from healthy tissue in their abnormal physiology and growth. Affected areas undergo changes in cell size and structure as well as molecular composition. These altered characteristics allow for differentiation, because they affect the physical properties of the tissue as a whole such as elasticity parameters or electric behavior. The latter can be investigated by the method of electrical impedance spectroscopy (EIS), which determines the complex impedance of tissue by applying an alternating voltage of various frequencies and measuring the resulting current, or vice versa. Impedance measurements can provide valuable information when investigating biological tissues and have so far been successfully used for tumor detection and tissue differentiation in various organs and applications [3]–[11].

One possible method to obtain impedance measurements consists of pushing needle probes into the tissue. This method delivers especially trustworthy results because it does not depend heavily on applied force and fluids on the tissue surface such as blood or non-conductive solutions. The measurements represent the inside of the tissue at a defined depth. However, when it comes to tumorous tissue, inserting into the affected area during *in vivo* measurements is not an option due to possible cancerous cell spreading. Noninvasive impedance sensors that are only held against the suspicious section and do not penetrate the tissue are necessary, but also more prone to exterior influences and errors.

Even though much progress has been made in the last few decades, the EIS measurement setups and methodologies are often inconsistent and it can happen that not enough detailed information about the experimental procedure is available. This results in difficulty when trying to reproduce or interpret results, especially when only absolute measured impedances instead of tissue related values are provided. Indeed, consistent and valid measurements and data post-processing routines are crucial to allow reproducible tissue differentiation. The aim of this work is to present different methods to determine the sensor specific geometry factor that connects absolute impedance data to material properties. This helps to establish a methodology to validate impedance sensors with distinct electrode arrangements and to assess the variance in impedance measurements for different sensors.

This work is structured as follows. At first, the fabrication and geometry of the examined sensors is presented. Afterwards, their geometry factors are determined by calculation,

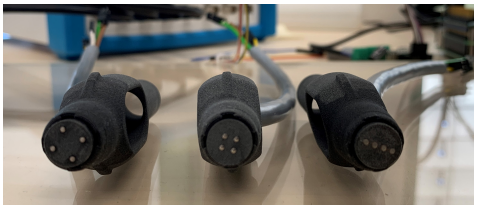

Fig. 1. 3D printed impedance sensor probes.

This work was conducted in the framework of the Graduate School 2543/1 "Intraoperative Multisensory Tissue Differentiation in Oncology" (project ID 40947457) funded by the German Research Foundation (DFG - Deutsche Forschungsgemeinschaft)

[1] Institute for System Dynamics, University of Stuttgart {veil, somers, sawodny, tarin}@isys.uni-stuttgart.de

simulation, and experimentally. Measurements on stored and fresh pig bladders are taken to validate the results. A discussion of the outcomes concludes the work.

II. Impedance Measurement and Sensors

The electrical impedance $\underline{Z}$ is a frequency-dependent, complex parameter, which is described by

$$\underline{Z} = \frac{\underline{u}(\omega)}{\underline{i}(\omega)} = R + jX, \tag{1}$$

with $\underline{Z}$ in Ω, alternating voltage $\underline{u}$ and current $\underline{i}$ of frequency ω as well as resistance R and reactance X.

A major part of consistent impedance measurements is a suitable sensor. If no specific requirements are demanded, such as a very small size or use of medically approved materials, an adequate sensor can be manufactured easily when considering only certain aspects, namely number of electrodes and material. A problem of electrode polarization occurs due to varying mobility of electronic and ionic charge carriers at the tissue-sensor-interface [12]. This effect can be mitigated through the use of suitable electrode materials such as stainless steel, platinum, or gold. It can be further diminished by implementing a four terminal measurement. This refers to using separate pairs of electrodes for carrying the current and measuring the voltage [13].

The impedance sensors in this work are made by 3D-printing a case of Nylon (PA12) and placing four stainless steel dowel pins of $1\,\mathrm{mm}$ diameter and $12\,\mathrm{mm}$ length in the respective configuration. A total set of three probes is manufactured that are shown in Figure 1 and whose geometries are further specified in Figure 2. The first probe is based on the original linear four terminal measurement where the electrodes are placed inline on a circular probe surface of $10\,\mathrm{mm}$ diameter. For the two other probes, the electrodes are placed in a square and differ in their distance and subsequently the size of the square. Note that, even though the exterior case still has a diameter of $10\,\mathrm{mm}$, the effective sensor diameter is reduced to approximately $5\,\mathrm{mm}$ by the diminished spacing. According to the differences in electrode arrangement (row, square) and distancing, the sensors are referred to as R10, S10, and S5. After soldering the electrodes to coaxial cables, the probe tip is filled with epoxy resin to hold the electrodes in place and make the tip watertight.

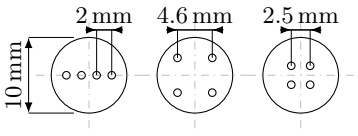

Fig. 2. Geometry of impedance sensors. Corresponding names from left to right: R10, S10, S5; based on electrode arrangement and effective outer diameter.

The *Zurich Instruments MFIA* Impedance Analyser (MFIA) with a frequency range from $1\,\mathrm{mHz}$ to $5\,\mathrm{MHz}$ is used to measure impedance. It uses a factory set internal calibration. In the setup, coaxial cables of $1\,\mathrm{m}$ length connect the probes to the MFIA. Each probe uses its own coaxial cables that are soldered the electrodes to connect to the MFIA cables. This is done to minimize unshielded portions of signal wire and maintain easy interchangeability of sensors for testing.

III. Geometry Factor Determination

When comparing different sensors with altered geometric properties, the comparison of simply the absolute impedance values is not an appropriate criterion. More precisely, in a four terminal measurement setup, the measured voltage does not only depend on the electrical properties of the tissue but also on the geometric characteristics of the sensor. This means that the measured voltage between the measurement electrodes is $\underline{u}_{\text{meas}}(\omega) = \underline{Z}_{\text{meas}}\underline{i}(\omega)$, with apparent impedance $\underline{Z}_{\text{meas}}$ between these electrodes and the injected current $\underline{i}(\omega)$. Normalizing the impedance to the geometry yields the impeditivity. Generally speaking, a term such as impedance depends on both electrical properties of the sample and the measuring setup and geometry. However, impeditivity encompasses only material constants, independent of external factors [13]. This applies for all quantities in the area of electrical properties, such as conductance, or admittance. The impedivity $\underline{z}$, resistivity ρ, and reactivity x can be calculated from the apparent impedance $\underline{Z}_{\text{meas}}$ by a constant k, which is often called geometry factor or probe constant. It is

$$\underline{z} = \frac{\underline{Z}_{\text{meas}}}{k} = \frac{R_{\text{meas}}}{k} + j\frac{X_{\text{meas}}}{k} = \rho + jx, \tag{2}$$

with $\underline{z}$, ρ, and x in $\Omega\,\mathrm{m}$, and geometry factor k in m^{-1}. The adequate determination of this sensor specific constant k is crucial for correct and reproducible impedance measurements on tissue. In the following, different procedures to obtain the geometry factor are presented. All resulting values are compared in Table I and Figure **??**.

A. Calculation

When looking at the direct current case, analytical equations for certain sensor geometries, especially for the usage of point electrodes, can be derived. According to the real part of (2), the apparent resistance is linked to the actual resistivity ρ of the examined object as $R_{\text{meas}} = k\rho$. By deriving an expression for V_{meas} and using Ohm's law, i.e. $V_{\text{meas}} = R_{\text{meas}}I$, it is possible to determine the geometry factor as

$$k = \frac{V_{\text{meas}}}{\rho I}. \tag{3}$$

Next, consider the general Laplace equation

$$\nabla^2 V = 0, \tag{4}$$

which states the potential equation for a field free of space charge [14]. A solution to Laplace's equation assuming boundary conditions of an infinite isotropic homogeneous medium,

$$V = \frac{I\rho}{2\pi r}, \tag{5}$$

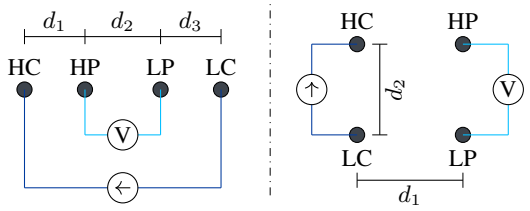

Fig. 3. Electrode arrangements and measurement setup inline (left) and as a rectangle (right).

allows for determining the potential V at any point inside the medium caused by a small current source I and evaluated at a distance r from this source [15].

The notation in the following is corresponds with Figure 3. The current-injecting electrode is referred to as high current (HC), the current sink electrode as low current (LC). Analogously, the potential electrodes are called low potential (LP) and high potential (HP). Assuming the electrodes as point sources and sinks, the aim is to find an analytical expression for the potential V_{meas} by evaluating (5) between the measurement electrodes LP and HP, and infer k according to (3).

1) Electrodes in a Row: The voltage at the first measurement electrode

$$V_{\text{HP}} = \underbrace{\frac{I\rho}{2\pi d_1}}_{\text{from source HC}} - \underbrace{\frac{I\rho}{2\pi(d_2+d_3)}}_{\text{from sink LC}} \tag{6}$$

is composed of the potential driven by the current source in distance d_1 and the current sink in distance $d_2 + d_3$. In the same manner, it is

$$V_{\text{LP}} = \frac{I\rho}{2\pi(d_1+d_2)} - \frac{I\rho}{2\pi d_3}. \tag{7}$$

The difference between the two results in the measured voltage

$$V_{\text{meas}} = V_{\text{HP}} - V_{\text{LP}} = \frac{I\rho}{2\pi}\left(\frac{1}{d_1} - \frac{1}{d_1+d_2} + \frac{1}{d_3} - \frac{1}{d_2+d_3}\right), \tag{8}$$

which again can be inserted into (3). Finally, the geometry factor for the sensor geometry in row is given by

$$k_{\text{row}} = \frac{1}{2\pi}\left(\frac{1}{d_1} - \frac{1}{d_1+d_2} + \frac{1}{d_3} - \frac{1}{d_2+d_3}\right). \tag{9}$$

Assuming a symmetrical probe, or even equidistantly spaced electrodes with distances $d_i = d$ such as R10 from Figure 1, (9) simplifies to

$$k_{\text{row}} = \frac{1}{2\pi d}. \tag{10}$$

For the sensor R10, it is $d = 2\,\text{mm}$ and, therefore, $k_{\text{R10,calc}} = 79.58\,\text{m}^{-1}$. Littwitz demonstrated the same procedure in 1990 [16]; his result however differs by a factor of 2.

2) Electrodes in a Rectangle: When the electrodes are arranged in a rectangle according to Figure 3, the potentials at the measurement electrodes are

$$V_{\text{HP}} = \frac{I\rho}{2\pi d_1} - \frac{I\rho}{2\pi\sqrt{d_1^2+d_2^2}}, \tag{11}$$

$$V_{\text{LP}} = \frac{I\rho}{2\pi\sqrt{d_1^2+d_2^2}} - \frac{I\rho}{2\pi d_1}, \tag{12}$$

and, thus,

$$V_{\text{meas}} = \frac{I\rho}{\pi}\left(\frac{1}{d_1} - \frac{1}{\sqrt{d_1^2+d_2^2}}\right). \tag{13}$$

The geometry factor as in (3) for a sensor with electrodes placed in a rectangle yields

$$k_{\text{rect}} = \frac{1}{\pi}\left(\frac{1}{d_1} - \frac{1}{\sqrt{d_1^2+d_2^2}}\right). \tag{14}$$

Assuming the electrodes are placed in a square, then $d = d_1 = d_2$ and the geometry factor is simplified to

$$k_{\text{square}} = \frac{1}{\pi d}\left(1 - \frac{1}{\sqrt{2}}\right). \tag{15}$$

For the sensor S10, it is $d = 4.6\,\text{mm}$ and, consequently, $k_{\text{S10,calc}} = 20.27\,\text{m}^{-1}$. With a distance of $d = 2.5\,\text{mm}$, the geometry factor for sensor S5 is $k_{\text{S5,calc}} = 37.29\,\text{m}^{-1}$.

B. Simulation

For simulation, a material or solution with known isotropic electrical properties can be used as a dielectric. In this work, *ANSYS Electronics Desktop* serves as the simulation environment. This allows the determination of influencing factors of the sensor geometries via parametric models. The *Maxwell DC-Conduction* solver is used to determine the voltage during current injection and, hence, the impedance.

1) Setup: The simulation setup was designed such that it reflects the experimental setup used for validation. The conductivity of the dielectric is set to $1413\,\mu\text{S}\,\text{cm}^{-1}$. A parameter study showed that the lateral expansion has little influence on the impedance if there is a certain distance between the electrodes and the edge of the dielectric. It also showed that no changes in simulated impedance occur with a thickness of the dielectric beneath the sensor larger than $10\,\text{mm}$. Thus, the geometry of the simulated dielectric was chosen to be as closely as possible to the experimental setup as a cylinder with diameter $100\,\text{mm}$ and $15\,\text{mm}$ height. Isolating boundary conditions at the bottom and sides of the cylinder are used and the simulated electrodes (stainless steel dowel pins) are placed in air against the dielectric cylinder. Perfect contact is assumed.

2) Simulation Results: A current of $100\,\mu\text{A}$ is applied to one current-carrying electrode and discharged via the second. The measuring electrodes are assumed to be floating, since the voltage is to be tapped at these with a very high impedance. As expected, the simulation shows a change in resulting resistance and thus in the geometry factor for the different sensors. The more cross-sectional area available between the electrodes, the lower the resistance. Most importantly, the spacing of the electrodes is critical to the probe's geometry factor. The simulation results in $k_{\text{R10,sim}} = 80.95\,\text{m}^{-1}$, $k_{\text{S10,sim}} = 20.66\,\text{m}^{-1}$, and $k_{\text{S5,sim}} = 37.78\,\text{m}^{-1}$. Furthermore, by evaluating the simulation, it is possible to determine not only the geometry factor but also how deep currents penetrate into the tissue and which current densities are reached. The simulated current densities are depicted in Figure 4.

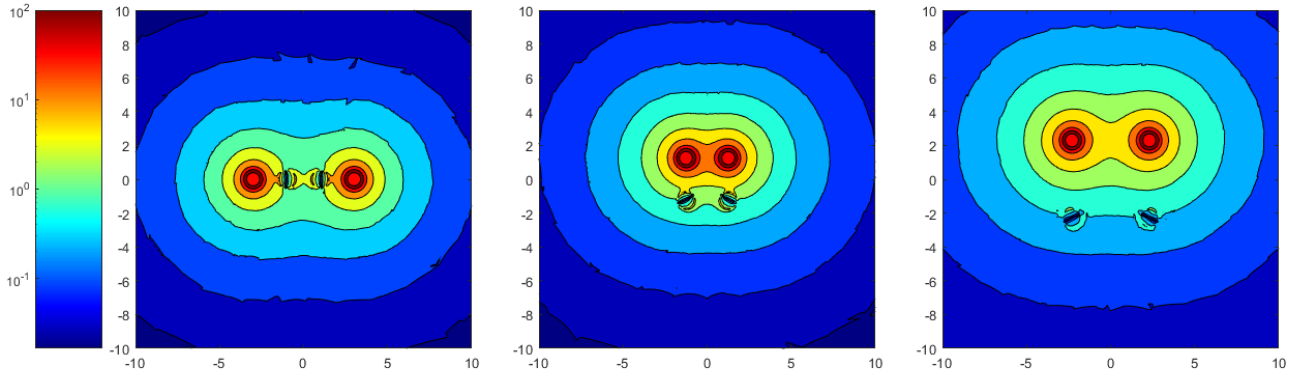

Fig. 4. The current density at the surface of a dielectric of $\sigma = 1413\,\mu\mathrm{S\,cm^{-1}}$ with R10 (left), S5 (middle) and S10 (right). In this case $100\,\mu\mathrm{A}$ are applied with isolating boundary condition on bottom and walls of the solution. The contours show the current density in a logarithmic scale from $0.01\,\mathrm{A\,m^{-2}}$ to $100\,\mathrm{A\,m^{-2}}$ and the surface is of size $10\,\mathrm{mm} \times 10\,\mathrm{mm}$, covering the physical sensor contact surface.

C. Experimental Determination

Experimentally, it is common to use a solution with known conductivity for calibration. The conductivity

$$\sigma = \frac{1}{\rho}, \tag{16}$$

is the inverse of resistivity and is measured in $\mathrm{S\,m^{-1}}$. The link to resistance and impedance is established as shown in (2). Hence, when measuring the calibration solution with known conductivity σ, the geometry factor k is obtained from the measured resistance R_{meas} by

$$k_{\mathrm{exp}} = R_{\mathrm{meas}}\sigma. \tag{17}$$

In the presented experiment, the impedance of a commercial calibration solution with conductivity $\sigma_{\mathrm{KCl}} = 1413\,\mu\mathrm{S\,cm^{-1}}$ at $25\,^{\circ}\mathrm{C}$ was measured with each sensor. It was filled $15\,\mathrm{mm}$ high into a round beaker with $100\,\mathrm{mm}$ diameter. Such solutions do not exhibit major dispersion for frequencies below the MHz range [17]. The relatively constant resistance for frequencies between $1\,\mathrm{kHz}$ and $10\,\mathrm{kHz}$ is shown in Figure 5 and averaged in order to determine a mean resistance R_{m}. With this value, it is possible to obtain the geometry factors according to (17), resulting in $k_{\mathrm{R10,exp}} = 73.63\ \mathrm{m^{-1}}$, $k_{\mathrm{S10,exp}} = 23.17\,\mathrm{m^{-1}}$, and $k_{\mathrm{S5,exp}} = 33.17\,\mathrm{m^{-1}}$.

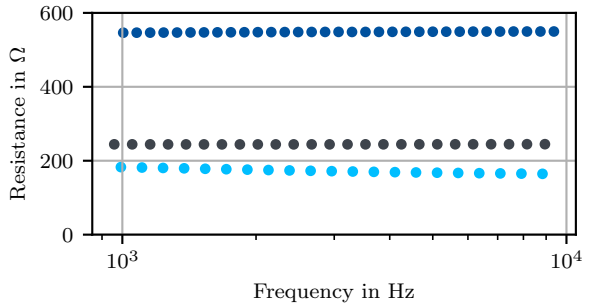

Fig. 5. Resistance measurement of conductivity calibration solution. R10: ▪▪▪▪ S10: ▪▪▪▪ S5: ▪▪▪▪

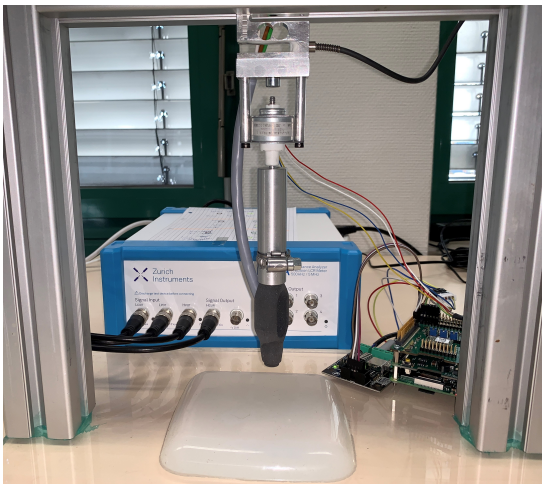

Fig. 6. Experimental setup: Impedance sensor probes mounted onto a testbench with linear actuator and force sensor, allowing to control and monitor sensor-tissue contact force.

IV. Measurements on Pig Bladders

Measurements on pig bladders are carried out in order to validate the sensors. The bladders are taken from fresh pig cadavers provided by the Urology Clinic, Tübingen, Germany. One portion was directly used to take measurements, and the other portion was put to frozen storage for several days.

The force with which the probe is pressed onto tissue cannot be easily controlled in a surgical setup. However, it is important to quantify its impact in order to understand

TABLE I
Overview of calculated, simulated and experimentally determined geometry factors in $\mathrm{m^{-1}}$

Sensor	Calculation	Simulation	Experiment
R10	79.58	80.95	73.63
S10	20.27	20.66	23.17
S5	37.29	37.78	33.17

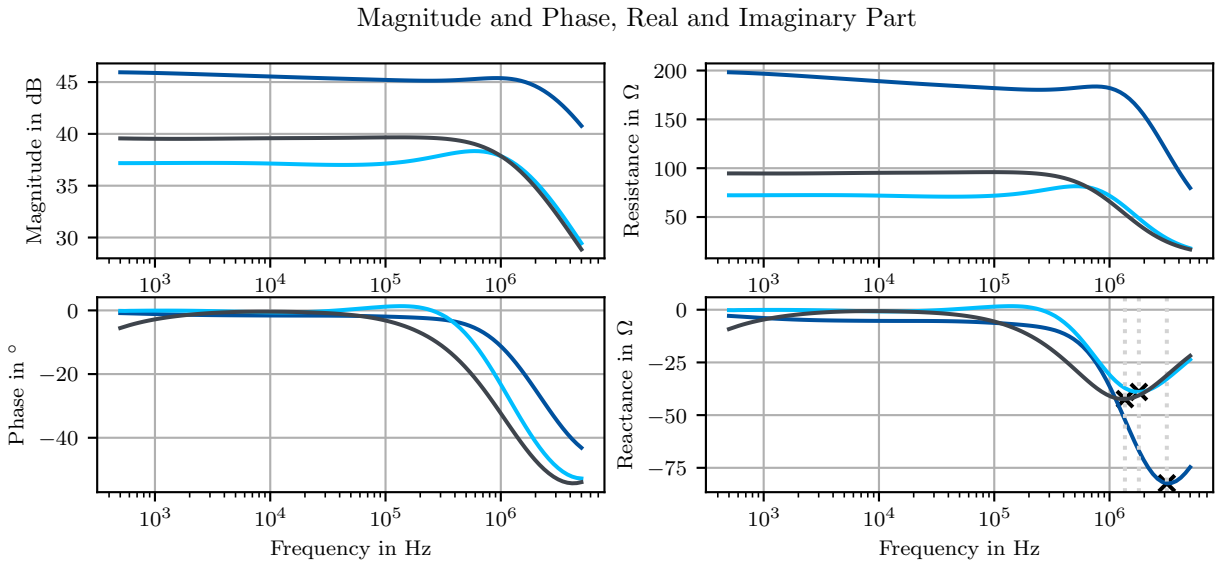

Fig. 7. Averaged measurement for each sensor. The characteristic frequencies f_c (×) are determined by the minimum of the imaginary part. R10: — S10: — S5: —

differences in the measured impedance when the force is not controlled. The sensors have a casing that can be mounted onto a test bench as depicted in Figure 6. A linear actuator and a force transducer are placed above that are connected with a Raspberry Pi Model 3B. Beneath the setup, the tissue is placed on an piece of silicone in order to imitate mechanical properties of underlying tissue and organs. All of the following measurements are carried out at a controlled contact force of 1 N to ensure good electrical contact.

Due to the different geometries of the sensors, the absolute impedance values differ approximately by the same factor as the geometry factors. Several measurements on two defrosted pig bladders are carried out and averaged for each sensor geometry. The Bode plot and the values of real and imaginary part are depicted in Figure 7. Due to the high amount of measurement points and the broad frequency spectrum, only the interpolation is plotted. Intuition leads to an expected difference in the magnitude and absolute values. However, likewise the dispersions occur at different frequencies f_c. In other words, the absolute value of the imaginary part peaks while the magnitude and phase start decreasing. In a Nyquist plot, this corresponds to the top of the circular arc. The characteristic time constant of the tissue is calculated by

$$\tau = \frac{1}{2\pi f_c} \tag{18}$$

from this critical frequency f_c. These values are listed in Table II.

Additional measurements are taken using fresh pig bladders, only a few hours after excision. The difference in the measured conductivity between fresh and defrosted tissues is depicted in Figure 8. According to [18], the conductivity of the human urinary bladder wall varies between $0.23\,\mathrm{S\,m^{-1}}$ and $0.26\,\mathrm{S\,m^{-1}}$ in the given frequency domain. With the assumption that human and pig bladder tissue does not differ significantly, this confirms that the measurements are valid. Moreover, increased conductivity, corresponding to diminished resistivity, is perceived after defrosting the tissue.

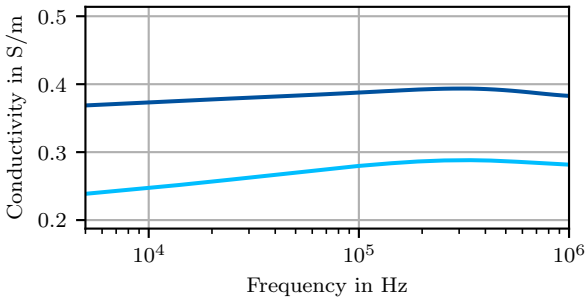

Fig. 8. Averaged measurements with sensor R10 on freshly excised and defrosted pig bladders. Defrosted: — Fresh: —

V. Discussion

The geometry factors obtained by calculation with (10) and (15) and the ones determined in simulation are in agreement with one another, resulting in effectively the same values. The slight discrepancy might lie in the fact that the calculation ignores the electrode surfaces, assuming point current sources and sinks, and point voltage measurements.

TABLE II
Characteristic Values of Different Sensors

Sensor	critical frequency f_c	time constant τ
R10	3.14 MHz	51 ns
S10	1.80 MHz	88 ns
S5	1.36 MHz	117 ns

The smaller k obtained with the calculation indicates less resistance between the voltage electrodes because the resistance of the point electrodes is negligible in comparison to actual planar electrodes with a surface of $A_{\mathrm{el}} = 0.79\,\mathrm{mm}^2$. This could also be one of the reasons why the experimentally derived factors differ from the numerical results. The experimentally determined parameter k_{exp} is about $10\,\%$ smaller for the sensors R10 and S5 but for S10 it is $12\,\%$ larger, deviating from the theoretical values. This can be linked to uncertainty in the solution mixture, general human error during measuring and unknown or not monitored effects such as temperature changes or tremor. It is deemed reasonable to use calculated or simulated geometry factors for future work. However, one should keep in mind that the presented model does not represent possible effects due to the connections after the electrodes and surface contact conditions.

Another important insight concerns the arrangement of the electrodes. It is apparent that, even though the inline layout is the suggested geometry in literature for four terminal measurements, the impedance data obtained with electrodes with a square arrangement is also valid. The absolute values are smaller, but, after normalization, result in comparable material specific values.

VI. Conclusion and Future Work

Three different methods to determine the geometry factor of tetrapolar impedance sensors were presented. The calculation via Laplace's equation, assuming point current sources and sinks yields the same results as the FEM setup. The experimentally determined values differ but lie within a reasonable range. Furthermore, a measurement setup for tissue differentiation based on EIS was established, including the manufacturing of measurement probes with different sensor geometries. The sensors were tested on both defrosted and fresh pig bladders and yielded conductivity values in the expected range.

It is now crucial to transfer the sensor principle to smaller geometries that are suitable for the special case of bladder cancer and transurethral diagnostics. The square arrangement is more advantageous for space saving implementations because it can be made smaller in diameter with the same electrode surface. Another potential means of diminishing the area further is by shrinking the voltage measuring electrodes while enlarging the current injecting electrodes to help maintain the current density. Overall, the simulation is an especially convenient tool since it facilitates the geometry factor determination before the actual production. Hence, it allows an investigation and possible optimization before the fabrication and allow to determine the geometry factor for more complicated electrodes such as ring electrodes. Due to the enormous computational effort involved, it is currently not feasible to perform a numerical simulation model of an EIS test setup at tissue cell level. The aspect ratio between the cell membrane, which is on the order of a few nanometers, and the distance between the electrodes, which is a few millimeters, is too large for simulations to be practical. However, the homogeneous material could be exchanged in simulation with a simplified layered model of the tissue and also compared with experimental data.

References

[1] "American Cancer Society - bladder cancer." https://www.cancer.org/cancer/bladder-cancer.html, accessed: 2020-11-27.

[2] J. A. Witjes, J. P. Redorta, D. Jacqmin, F. Sofras, P.-U. Malmström, C. Riedl, D. Jocham, G. Conti, F. Montorsi, H. C. Arentsen *et al.*, "Hexaminolevulinate-guided fluorescence cystoscopy in the diagnosis and follow-up of patients with non–muscle-invasive bladder cancer: review of the evidence and recommendations," *European urology*, vol. 57, no. 4, pp. 607–614, 2010.

[3] V. S. Teixeira, V. Labitzky, U. Schumacher, and W. Krautschneider, "Use of electrical impedance spectroscopy to distinguish cancer from normal tissues with a four electrode terminal setup," *Current Directions in Biomedical Engineering*, vol. 6, no. 3, pp. 341–344, 2020.

[4] V. S. Teixeira, W. Krautschneider, and J. J. Montero-Rodríguez, "Bioimpedance spectroscopy for characterization of healthy and cancerous tissues," in *2018 IEEE International Conference on Electrical Engineering and Photonics (EExPolytech)*. IEEE, 2018, pp. 147–151.

[5] H. M. Fahmy, A. M. Hamad, F. A.-z. Sayed, Y. S. Abdelaziz, E. S. Abu Serea, A. B. E.-D. Mustafa, M. A. Mohammed, and A. M. Saadeldin, "Dielectric spectroscopy signature for cancer diagnosis: A review," *Microwave and Optical Technology Letters*, vol. 62, no. 12, pp. 3739–3753, 2020.

[6] F. Simini and P. Bertemes-Filho, *Bioimpedance in biomedical applications and research*. Springer, 2018.

[7] S. L. Hillary, B. H. Brown, N. J. Brown, and S. P. Balasubramanian, "Use of electrical impedance spectroscopy for intraoperative tissue differentiation during thyroid and parathyroid surgery," *World Journal of Surgery*, vol. 44, no. 2, pp. 479–485, 2020.

[8] J. Wu, P. Wang, Y. Tang, H. Liu, H. Wang, W. Zhang, Y. Zhang, L. Chen, Z. Xu, and X. Yao, "A new method to rapidly identify benign and malignant breast lumps through bioelectrical impedance spectroscopy," *Medical physics*, vol. 46, no. 5, pp. 2522–2525, 2019.

[9] S. M. Moqadam, P. K. Grewal, Z. Haeri, P. A. Ingledew, K. Kohli, and F. Golnaraghi, "Cancer detection based on electrical impedance spectroscopy: A clinical study," *Journal of Electrical Bioimpedance*, vol. 9, no. 1, p. 17, 2018.

[10] A. Pathiraja, P. Ziprin, A. Shiraz, R. Mirnezami, A. Tizzard, B. Brown, A. Demosthenous, and R. Bayford, "Detecting colorectal cancer using electrical impedance spectroscopy: an ex vivo feasibility study," *Physiological measurement*, vol. 38, no. 6, p. 1278, 2017.

[11] S. Shetty, U. Anushree, R. Kumar, and S. Bharati, "Electrical conductivity spectra of hepatic tumors reflect hepatocellular carcinoma progression in mice," *Biomedical Physics & Engineering Express*, vol. 6, no. 6, p. 065019, 2020.

[12] B. Singh, C. Smith, and R. Hughes, "In vivo dielectric spectrometer," *Medical and Biological Engineering and Computing*, vol. 17, no. 1, pp. 45–60, 1979.

[13] S. Grimnes and O. Martinsen, *Bioimpedance and Bioelectricity Basics*. Elsevier Science, 2014.

[14] K. Küpfmüller, *Einführung in die theoretische Elektrotechnik*, 5th ed. Springer-Verlag OHG, 1955.

[15] J. Jakosky, "Exploration geophysics," *Truth Publishers, Los Angeles, California*, pp. 186–187, 1940.

[16] C. Littwitz, T. Ragheb, and L. Geddes, "Cell constant of the tetrapolar conductivity cell," *Medical and Biological Engineering and Computing*, vol. 28, no. 6, pp. 587–590, 1990.

[17] A. Ruiz-Vargas, A. Ivorra, and J. W. Arkwright, "Design, construction and validation of an electrical impedance probe with contact force and temperature sensors suitable for in-vivo measurements," *Scientific reports*, vol. 8, no. 1, pp. 1–11, 2018.

[18] P. Hasgall, F. Di Gennaro, C. Baumgartner, E. Neufeld, B. LLoyd, M. Gosselin, D. Payne, A. Klingenboeck, and N. Kuster, "IT'IS database for thermal and electromagnetic parameters of biological tissues," May 2018, version 4.0, May 15, 2018. [Online]. Available: itis.swiss/database